

Synergistic Co-Recycling: Selective Oxidation of Polyethylene to Dicarboxylic Acids over Spent LiCoO₂ Cathodes

Shengming Li⁺, Qianye Feng⁺, Qingye Li⁺, Yeping Xie, Panpan Xu,* Zhao Wang, Qiming Sun, Muhan Cao, Qiao Zhang, and Jinxing Chen*

Abstract: The escalating production of lithium-ion batteries and plastics poses critical challenges to environmental integrity and resource sustainability. Here, we report a synergistic co-recycling strategy for spent lithium cobalt oxide (LCO) cathodes and waste polyethylene (PE), leveraging the catalytic properties of LCO to oxidize PE into high-value dicarboxylic acids. Through a combination of density functional theory calculations, electron spin resonance, and in situ infrared spectroscopy, we reveal that lithium-deficient LCO undergoes a spin-state transition of Co³⁺ to a high-spin state, facilitating the activation of oxygen and the generation of singlet oxygen. This reactive oxygen species drives the selective oxidation of PE via hydrogen atom transfer, achieving dicarboxylic acid yields of up to 77.5 wt%, markedly exceeding previous benchmarks. Validation with real-world plastic waste and spent batteries underscores the feasibility of this approach, presenting a sustainable paradigm-shift solution for the efficient management of lithium-ion batteries and plastic waste in a circular economy.

Introduction

The relentless growth in global plastic production, driven by escalating demand, has led to a parallel surge in plastic waste,

overwhelming existing recycling infrastructures.^[1–4] By 2050, it is projected that approximately 12 billion metric tons of plastic waste will accumulate in natural ecosystems, resulting in significant environmental challenges.^[5] Waste polyethylene (PE), accounting for approximately one-third of global plastic production, epitomizes this challenge due to its chemical inertness and resistance to degradation under mild conditions. Its robust C(sp³)–C(sp³) bonds, stabilized by a symmetrical electron cloud, create high thermodynamic barriers to cleavage, making PE recycling particularly difficult.^[6–11] Current recycling technologies are largely reliant on energy-intensive, high-temperature processes, which are economically and environmentally unsustainable.^[12–14]

To address these challenges, oxygen-assisted catalytic strategies have recently gained traction as a promising alternative for the selective upcycling of PE under milder conditions.^[15–20] These approaches exploit the exothermic nature of oxygen insertion into the carbon backbone to thermodynamically drive C–C bond cleavage through cascading reactions. Concurrently, the formation of carbon–oxygen radical intermediates disrupts the electron cloud symmetry around C–C bonds, promoting β -scission kinetics.^[21,22] For instance, Zhao et al.^[23] demonstrated a low-temperature, ambient-pressure oxidation system using a homogeneous catalyst to convert PE into carboxylic acids. Similarly, Xu et al.^[24] developed a stepwise process combining pyrolysis and oxidation to produce monocarboxylic acids suitable for soap production, while Wang et al.^[25] and Zhang et al.^[26] engineered catalysts to selectively yield dicarboxylic acids. These catalytic systems utilizing transition metal oxides (e.g., Co, Mn) have demonstrated the ability to convert PE into value-added oxygenated products through the formation of reactive oxygen species (ROS). Despite these advances, the reliance on specific transition metals raises sustainability concerns, particularly given the rising demand for cobalt and manganese in renewable energy technologies.


In parallel, the rapid growth of lithium ion batteries (LIBs) markets, driven by the proliferation of electric vehicles and stationary energy storage, has highlighted an urgent need to address battery waste streams.^[27–31] Lithium cobalt oxide (LCO)-based batteries, dominant in consumer electronics due to their high energy density and stability, represent a significant share of this waste.^[32–34] The disposal of spent LCO batteries not only leads to environmental contamination but also exacerbates the depletion of critical cobalt resources. Recycling LCO into functional catalytic materials offers a dual benefit, enabling resource circularity while mitigating

[*] S. Li⁺, Q. Feng⁺, Q. Li⁺, Y. Xie, M. Cao, Q. Zhang, J. Chen
 State Key Laboratory of Bioinspired Interfacial Materials Science,
 Institute of Functional Nano & Soft Materials (FUNSOM), Soochow
 University, Suzhou 215123, P.R. China
 E-mail: chenjinjing@suda.edu.cn

S. Li⁺, Q. Feng⁺, Q. Li⁺, Y. Xie, M. Cao, Q. Zhang, J. Chen
 Jiangsu Key Laboratory for Carbon-Based Functional Materials &
 Devices, Soochow University, Suzhou, Jiangsu 215123, P.R. China
 P. Xu
 Suzhou Institute of Nano-Tech and Nano-Bionics, Chinese Academy
 of Sciences, Suzhou, Jiangsu 215123, P.R. China
 E-mail: panpanxu2021@sinano.ac.cn

Z. Wang, Q. Sun
 College of Chemistry, Chemical Engineering and Materials Science,
 Soochow University, Suzhou, Jiangsu 215123, P.R. China

[⁺] These authors contributed equally to this work.

 Additional supporting information can be found online in the
 Supporting Information section

the carbon-intensive extraction of primary cobalt ores.^[35,36] For example, Zhao et al.^[37] have upcycled LCO into a Co_3O_4 catalyst, which was then used for the electrocatalytic conversion of ethylene glycol, a polyethylene terephthalate-derived compound. However, this approach required complex steps such as acid digestion, separation, and resynthesis to reconstruct catalysts, thereby completely altering the original battery materials.

In this study, we propose a synergistic “PE+LCO” co-upgrading strategy, which directly utilizes LCO electrodes from retired LIBs as integrated catalysts. Operating at 130 °C for 6 h, this system achieved an exceptional carbon yield of 77.5 wt% for dicarboxylic acid products. By integrating projected density of states (PDOS) analysis and in situ infrared spectroscopy, we uncovered a spin-state-driven structure–performance relationship governing the catalytic oxidation of PE and proposed a plausible reaction mechanism. This work not only demonstrates an efficient, environmentally friendly platform for simultaneously addressing PE and LCO waste streams but also provides critical insights into the design of advanced PE oxidation catalysts and the mechanistic foundations of their activity. These findings contribute to the development of sustainable catalytic technologies at the intersection of polymer upcycling and battery material recycling.

Results and Discussion

Concept of Co-Recycling: LCO-Catalyzed PE Oxidation

The concept of co-recycling “LCO+PE” leverages cathodes materials in spent LCO batteries as a resource for catalytic upcycling of PE (Figure 1a). Spent LCO batteries were dismantled, and the cathode materials were processed via straightforward methods, including ball milling and purification, to obtain LCO catalyst powder. The oxidative conversion of PE was conducted by physically mixing the LCO catalyst with PE with a catalyst-to-PE mass ratio of 1:10 in a stainless-steel reactor under 1.0 MPa O_2 at 130 °C for 6 h, yielding oxygenated chemicals. The gaseous products from the reaction were directly collected using gas bags and analyzed with gas chromatography (GC), while the liquid and solid products were combined with methanol for collection. The solid conversion was calculated based on the mass difference before and after the reaction, shown in experimental details (see details in supporting information).

A control experiment without catalysts was conducted to exam the direct PE oxidation, where the PE solid conversion is less than 5.0 wt%. In contrast, the addition of pristine LCO into the reaction system increased conversion to 80.2 wt%. The space-time yield (STY) rose dramatically from 1.7 $\text{mg}_{\text{PE}} \text{ h}^{-1}$ in the control group to 26.7 $\text{mg}_{\text{PE}} \text{ h}^{-1}$, underscoring the catalytic efficiency of catalysts in promoting oxidative conversion of PE plastics. The primary gaseous products, as detailed in Figure S1, are CO_2 and CO (collectively referred to as CO_x products), mainly originating from the over-oxidation of PE. When pristine LCO was used as the catalyst, the CO_x generation was 0.6 mmol

(Table S1), accounting for ~4.2 mol% of the total carbon. The low CO_x yield indicates that the main products for catalytic oxidation of PE are liquid chemicals. The liquid product was primarily composed of aliphatic carboxylic acids, as confirmed by Fourier transform infrared (FT-IR) spectroscopy (Figure S2) and ^1H NMR spectroscopy (Figure S3). The liquid product distribution was further characterized by gas chromatography-mass spectrometry (GC-MS), revealing that dicarboxylic acids dominated the composition (Figures S4–S6). Quantification of monocarboxylic acids using ^1H NMR spectroscopy (see Supporting Note 1) determined their molar ratio to be ~3.5 wt%. Heteronuclear single quantum coherence (HSQC) NMR provided additional insights into the product composition (Figure 1b). The strong correlations between the proton peak and carbon peak suggest the formation of succinic acid (2.6 ppm vs. 28.6 ppm, Figure S7) and glutaric acid (2.5 ppm vs. 27.5 ppm, Figure S8). Proton signals below 2.2 ppm indicated the presence of long-chain dicarboxylic acids, usually with a carbon length exceeding 5. These results are consistent with the GC-MS.

Quantitative analysis of dicarboxylic acids is challenging due to the strong interactions between carboxylic acids and chromatographic columns, which result in significant detection errors. To overcome this limitation, we employed a pretreatment method involving esterification of the dicarboxylic acid products, followed by quantitative analysis using GC-MS. The detailed procedure is provided in Supporting Note 2. As shown in Figure 1c, the liquid product distribution reveals that pristine LCO achieves a dicarboxylic acid yield of 48.2 wt%. We performed a carbon balance assessment on the reaction products, with the carbon mass of the liquid dicarboxylic acid being 82.2 mg, the carbon mass of the monocarboxylic acid being ~9.6 mg, and the carbon mass of CO_x being 7.2 mg, giving a carbon balance rate of 72.3%. The missing carbon footprint is likely due to PE molecules remaining on the catalyst and losses during the liquid product collection process.

Considering two critical parameters in reaction temperature and time, we systematically optimized the catalytic oxidation of PE to maximize solid conversion and liquid carboxylic acid yield. Reactions were conducted at varying times (3, 6, 9, and 12 h) and temperatures (110 °C, 120 °C, 130 °C, 140 °C, and 150 °C) (Figure 1d; Table S2). At 110 °C and 3 h, the solid conversion was only 5.0 wt%, increasing marginally to 12.0 wt% after 12 h. However, at temperatures above 120 °C, the solid conversion rate increased significantly with extended reaction time, suggesting a critical temperature threshold. This critical temperature likely facilitates the transition of PE into a molten state, reducing mass transfer limitations and enhancing catalytic activity. At 130 °C and 6 h, the solid conversion reached ~75.0 wt%, further increasing to ~95.0 wt% after 12 h. However, longer reaction times also led to higher production of low-value gaseous products (Figure S9). To balance solid conversion and product value, 130 °C and 6 h were identified as the optimal catalytic conditions for this process. Additionally, various catalyst-to-plastic feed ratios were screened to determine the optimal ratio (Figure S10).

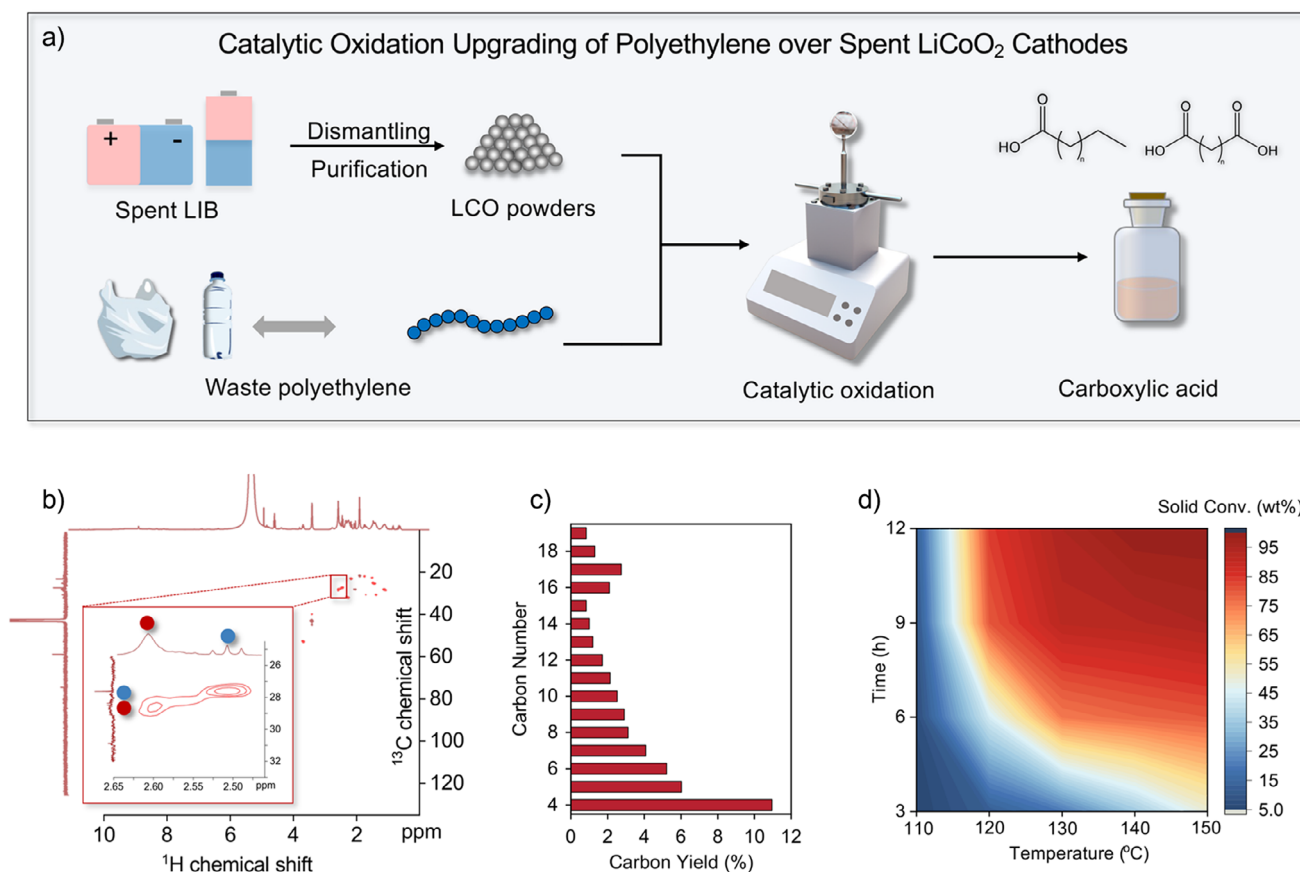


Figure 1. Co-recycling strategy of spent LCO and waste PE. a) Scheme for upgrading waste PE into carboxylic acid chemicals by catalytic oxidation of spent LCO. b) Aerobic catalytic oxidation of PE over pristine LCO catalysts. 2D HSQC NMR spectrum of liquid products using deuterated dichloromethane as solvent. Reaction conditions: $P(\text{O}_2) = 1.0 \text{ MPa}$, $T = 130 \text{ }^\circ\text{C}$, $t = 6 \text{ h}$, $m_{\text{catalyst}} = 20 \text{ mg}$, $m_{\text{PE}} = 200 \text{ mg}$. c) Carbon number distribution of dicarboxylic acid products over pristine LCO. d) Optimization of reaction temperature and time over pristine LCO. Reaction conditions: $P(\text{O}_2) = 1.0 \text{ MPa}$, $m_{\text{catalyst}} = 50 \text{ mg}$, $m_{\text{PE}} = 500 \text{ mg}$.

Li-Deficiency Effect on Catalytic Performance

The catalytic results demonstrate that pristine LCO exhibits superior catalytic activity. Given that real-world LCO batteries exist in various states of retirement, it is crucial to understand the relationship between the degree of delithiation and catalytic performance in PE oxidation to optimize recycling strategies. We employed controlled chemical delithiation to simulate LCO in different retired states (Figure 2a). LCO was chemically delithiated in a 0.2 M $\text{K}_2\text{S}_2\text{O}_8$ solution at 60 $^\circ\text{C}$ with varying times. The particle size remained largely unchanged during the delithiation process (Figures S11 and S12). The Li/Co ratio of the catalysts at different delithiation durations was quantified by inductively coupled plasma optical emission spectroscopy (ICP-OES, Figure 2b). The catalysts were categorized as follows based on their Li/Co ratios: $\text{Li}_{0.72}\text{CoO}_2$ (2 h), $\text{Li}_{0.62}\text{CoO}_2$ (4 h), $\text{Li}_{0.45}\text{CoO}_2$ (8 h), and $\text{Li}_{0.28}\text{CoO}_2$ (24 h).

The catalytic performance of $\text{Li}_{1-x}\text{CoO}_2$ catalysts with varying lithium deficiencies was further investigated. As shown in Figure 2c, increasing lithium removal led to a marked improvement in PE oxidation catalysis. The solid

conversion rate of PE increased from 80.0 wt% for pristine LCO to nearly 100 wt% for $\text{Li}_{0.28}\text{CoO}_2$, demonstrating the enhanced catalytic activity of lithium-deficient $\text{Li}_{1-x}\text{CoO}_2$. Additionally, lithium removal significantly boosted the carbon yields of liquid and gaseous products. The liquid product yield increased from 48.2 wt% with pristine LCO to 77.5 wt% with $\text{Li}_{0.28}\text{CoO}_2$, while the gaseous product yield increased from 4.0 wt% to 21.2 wt%. Carbon number distribution analysis of the liquid products (Figures 2d and S13) revealed a predominance of short-chain dicarboxylic acids ($C < 10$). These results suggest that lithium deficiency in the LCO catalyst lattice enhances oxygen activation, leading to the generation of more short-chain dicarboxylic acids. For example, when $\text{Li}_{0.28}\text{CoO}_2$ is employed as the catalyst, the product distribution is predominantly composed of succinic acid, glutaric acid, and adipic acid (C_4 – C_6), with these three products collectively exhibiting a selectivity of 81.8% (Figure 2d). These intermediates are valuable for pharmaceutical synthesis and hold substantial economic potential. Notably, the cathode materials of retired LCO batteries are often lithium deficient, and their direct use as catalysts for PE oxidation outperforms newly purchased LCO catalysts. This underscores the effectiveness of utilizing

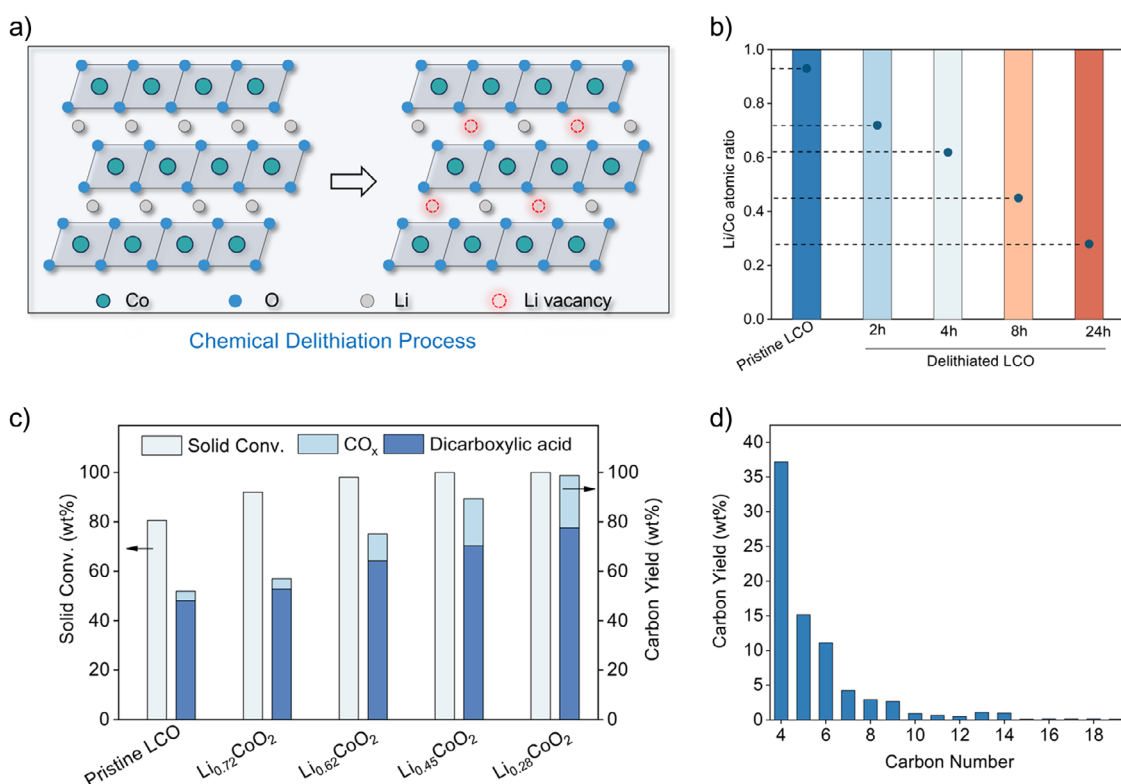


Figure 2. Performance optimization and structure-activity relationship of PE oxidation over $\text{Li}_{1-x}\text{CoO}_2$ Catalysts. a) Schematic diagram of the delithiation process. b) Li/Co molar ratios in pristine LCO and chemical delithiation treatment for different times. c) Catalytic oxidation of PE over $\text{Li}_{1-x}\text{CoO}_2$ catalyst. Reaction conditions: $P(\text{O}_2) = 1.0 \text{ MPa}$, $T = 130^\circ\text{C}$, $t = 6 \text{ h}$, $m_{\text{catalyst}} = 20 \text{ mg}$, $m_{\text{PE}} = 200 \text{ mg}$. d) Carbon number distribution of dicarboxylic acid products over $\text{Li}_{0.28}\text{CoO}_2$ catalyst. Reaction conditions: $P(\text{O}_2) = 1.0 \text{ MPa}$, $T = 130^\circ\text{C}$, $t = 6 \text{ h}$, $m_{\text{catalyst}} = 20 \text{ mg}$, $m_{\text{PE}} = 200 \text{ mg}$.

waste materials to treat other waste streams, highlighting a sustainable approach to catalysis and recycling.

Catalytic Mechanism

To elucidate the differences in catalytic performance between various $\text{Li}_{1-x}\text{CoO}_2$ catalysts, we conducted an electronic structure analysis of pristine LCO and severely lithium-deficient $\text{Li}_{0.28}\text{CoO}_2$. As shown in Figure 3a–c, delithiation caused the Co absorption edge to shift to higher energies in Co K-edge X-ray absorption near-edge structure (XANES) spectroscopy, indicating an increase in core electron, which reflects reduced interactions between O 2p orbitals and Co 3d orbitals. Furthermore, the peak near 7729 eV, related to Co oxidation states and edge energy, also shifts, highlighting changes in Co's local electronic structure during delithiation.

X-ray photoelectron spectroscopy (XPS) analysis further confirms the above conclusions. As shown in Figure 3d, the pristine catalyst predominantly contains Co^{3+} species with a binding energy of 778.6 eV. With increasing lithium deficiency, the Co binding energy shifts upward, indicating a partial transition to $\text{Co}^{\delta+}$ ($\delta > 3$). According to classical crystal field theory, Co^{3+} in LiCoO_2 is stabilized in a typical octahedral field under a low-spin state with an electron configuration of $e_g^0 t_{2g}^6$.^[38,39] Spin-polarized DFT calculations reveal that the lattice field strength weakens in $\text{Li}_{0.28}\text{CoO}_2$, decreasing from

−306.4 eV in the pristine material to −262.5 eV (Figure S14 and Table S3). This weakening is attributed to the formation of lithium vacancies. The reduction in lattice field strength favors the stabilization of Co^{3+} in a high-spin state under the weak field effect.

We performed PDOS calculations on pristine LCO and $\text{Li}_{0.28}\text{CoO}_2$, as shown in Figure 3e,f. For the pristine catalyst, the PDOS of the t_{2g} and e_g orbitals exhibits symmetry between spin-up and spin-down states around $y = 0$, indicating nonmagnetic behavior. Additionally, the t_{2g} orbitals display a higher density of states compared to the e_g orbitals below the Fermi level, suggesting that the t_{2g} orbitals dominate the stable electronic configuration. In contrast, the PDOS for $\text{Li}_{0.28}\text{CoO}_2$ reveals an asymmetry between spin-up and spin-down states for both t_{2g} and e_g orbitals, indicating the emergence of paramagnetic behavior. This transition is attributed to lattice distortions induced by lithium vacancies within the octahedral coordination of six oxygen atoms, which weaken the crystal field effect. Consequently, the six 3d electrons of Co^{3+} can adopt a high-spin configuration, with two unpaired electrons distributed across both t_{2g} and e_g orbitals. These findings suggest that lithium deficiency triggers a spin-state transition in Co^{3+} to a high-spin state, which may enhance its susceptibility to oxygen adsorption. This conclusion is further supported by the results of O_2 -TPD analysis. As shown in Figure 3g, the pristine LCO exhibits a characteristic physical oxygen desorption peak

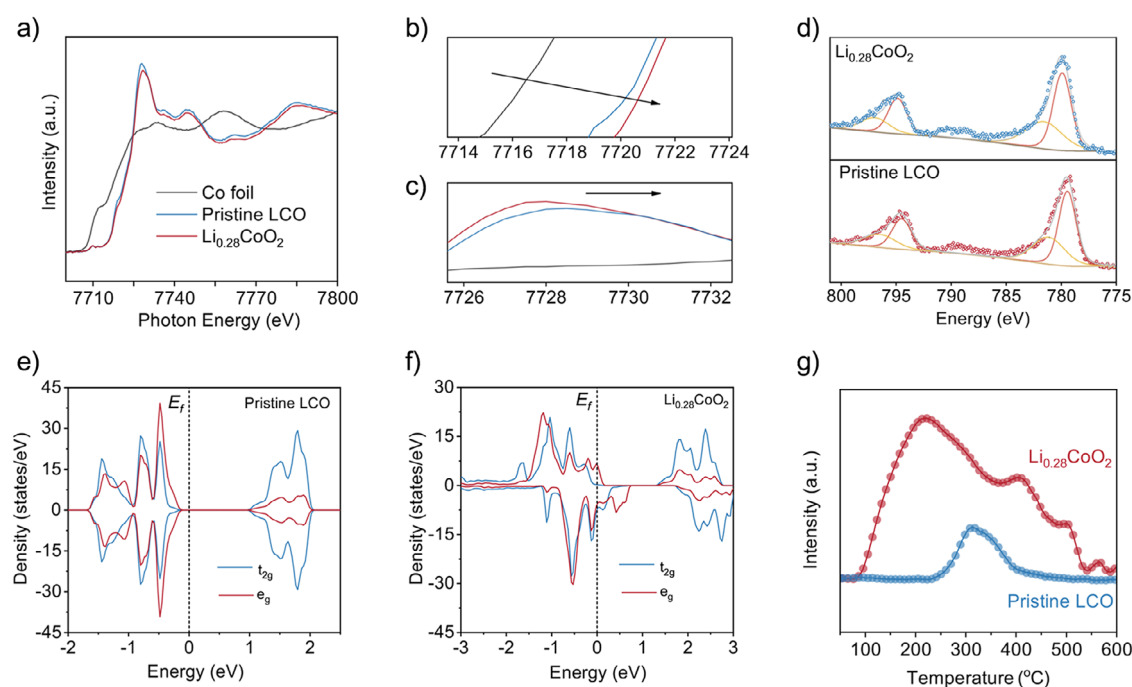


Figure 3. Electronic structure characterization of catalysts. a–c) XANES spectra of Co K-edge in pristine LCO, $\text{Li}_{0.28}\text{CoO}_2$, and Co foil. d) XPS spectra of pristine LCO and $\text{Li}_{0.28}\text{CoO}_2$. e, f) PDOS calculation spectrum of pristine LCO e) and $\text{Li}_{0.28}\text{CoO}_2$ f). g) O_2 -TPD spectra of pristine LCO and $\text{Li}_{0.28}\text{CoO}_2$ catalyst.

at $\sim 200^\circ\text{C}$, indicative of weak interactions with oxygen. In contrast, $\text{Li}_{0.28}\text{CoO}_2$ displays distinct chemical adsorption peaks at higher temperatures, specifically $\sim 420^\circ\text{C}$ and $\sim 500^\circ\text{C}$, suggesting a significantly stronger oxygen adsorption capacity. These observations indicate that the high-spin Co species, formed due to lithium vacancies, have an enhanced ability to adsorb oxygen. This improved oxygen adsorption capacity is likely a critical factor in boosting the catalytic performance of $\text{Li}_{0.28}\text{CoO}_2$ in oxidation reactions as the stronger interaction with oxygen facilitates more effective activation and subsequent oxidation processes.

To gain deeper insights into the mechanism of oxidative catalysis, we analyzed how cobalt oxides activate O_2 during the process. We first designed control experiments to investigate whether lattice oxygen would directly participate in the catalytic reaction (Figure S15). An impressive $\sim 95\text{ wt}\%$ HDPE conversion was achieved with only 20 mg $\text{Li}_{0.28}\text{CoO}_2$ at 1.0 MPa O_2 . In contrast, when O_2 was excluded with N_2 or Ar, no plastic conversion was observed even with excess catalysts were added to mimic lattice oxygen catalysis. Gel permeation chromatography (GPC) analysis of the remaining solid (Table S4) showed no significant decrease in PE molecular weight under a non-oxygen atmosphere. These findings indicate that the direct participation of lattice oxygen in metal oxides may be negligible at lower reaction temperatures, possibly due to stabilizing Co–O bonds in the LCO structure.^[40–42]

We used 2,2,6,6-tetramethylpiperidine (TEMP) and 5,5-dimethyl-1-pyrrolidine-N-oxide (DMPO) as scavengers for $^1\text{O}_2$, $\cdot\text{OH}$, and $\cdot\text{O}_2^-$, respectively, to investigate the types of reactive oxygen species involved in the catalytic reaction. As indicated in Figure 4a, a clear triplet signal attributed

to $^1\text{O}_2$ was observed in the electron paramagnetic resonance (EPR) spectrum, whereas no significant signals relating to $\cdot\text{OH}$ and $\cdot\text{O}_2^-$ were detected. These results suggest that $^1\text{O}_2$ is the primary ROS in the catalytic system. Additionally, the importance of $^1\text{O}_2$ in the reaction was underscored by adding $^1\text{O}_2$ scavenger of β -carotene, which reduced the yield of dicarboxylic acid decreased from 77.5 to 20.0 wt% (Figure S16). To evaluate the oxygen activation ability of $\text{Li}_{0.28}\text{CoO}_2$ and pristine LCO, EPR measurements were conducted (Figure 4b). $\text{Li}_{0.28}\text{CoO}_2$ exhibited a significantly stronger $^1\text{O}_2$ signal compared to pristine LCO, indicating its superior ability to activate oxygen. The observed difference in oxygen activation ability between $\text{Li}_{0.28}\text{CoO}_2$ and pristine LCO may be attributed to the spin state of cobalt. Higher-spin cobalt species are generally more effective at interacting with O_2 as a π -donor, thereby facilitating the activation of ground-state $^3\text{O}_2$ to excited-state $^1\text{O}_2$ (Figure 4c). This mechanism is also reflected in the control experiment. When Co_3O_4 was added as catalyst, the solid conversion and dicarboxylic acid carbon yield were 78.1 wt% and 52.5 wt%, respectively (Figure S17), which are comparable to these of the original LCO (80.5 wt% solid conversion, 48.1 wt% dicarboxylic acid yield), but significantly lower than the values of delithiated $\text{Li}_{0.28}\text{CoO}_2$ catalyst (100 wt% solid conversion, 77.5 wt% dicarboxylic acid yield). In addition, the $^1\text{O}_2$ signals of both catalysts increased with increasing reaction temperature (Figure 4b), indicating that the increased temperature can enhance the activation of inert O_2 . This temperature-dependent behavior underscores the importance of thermal energy in overcoming the activation barrier for oxygen excitation and highlights its role in enhancing the overall catalytic efficiency. To

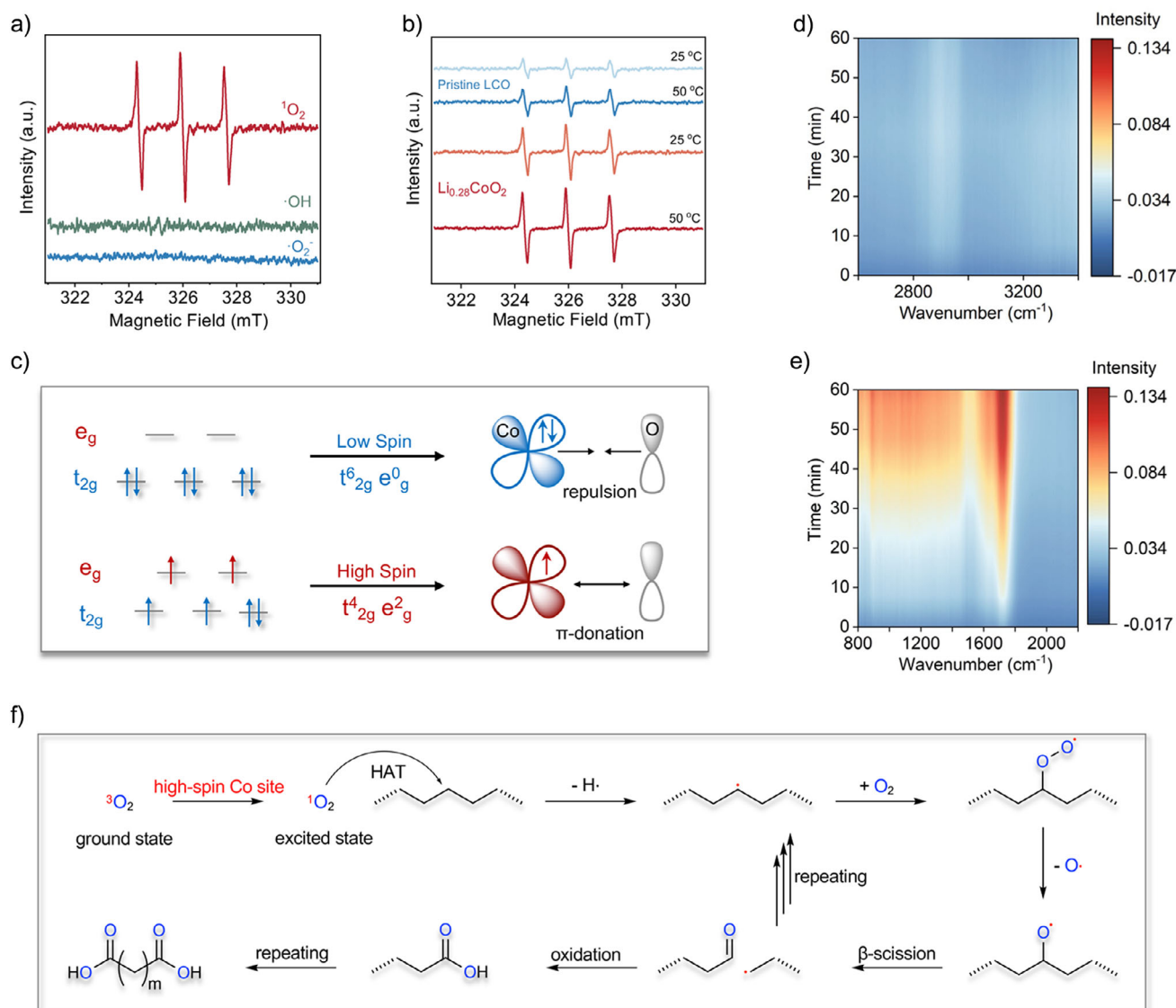


Figure 4. Catalytic oxidation mechanism. a) EPR signals of superoxide radical, singlet oxygen radical, and hydroxyl radical in the presence of $\text{Li}_{0.28}\text{CoO}_2$ at 25 °C (TEMP aqueous solution for capture of $^1\text{O}_2$. DMPO aqueous solution and methanol solution for capture of $\cdot\text{OH}$ and $\cdot\text{O}_2^-$). b) EPR signals of singlet oxygen radicals with pristine LCO and $\text{Li}_{0.28}\text{CoO}_2$ at 25 °C and 50 °C. c) Schematic diagram of electronic coupling of $\text{Co}^{3+}-\text{O}$ in high-spin and low-spin states. d, e) 2D in situ IR contour plot of HDPE oxidation catalyzed by $\text{Li}_{0.28}\text{CoO}_2$ oxidation at 250 °C in atmospheric air with different spectrum ranges. f) Possible mechanism diagram of $\text{Li}_{1-x}\text{CoO}_2$ -catalyzed PE oxidation.

investigate the oxygen-initiated conversion of PE to dicarboxylic acids over LCO, we performed in situ infrared spectroscopy to monitor the reaction process (see experiment section). As shown in Figure 4d, the C–H stretching signals at 2900–3000 cm^{-1} remained unchanged during the reaction, indicating a low PE conversion rate within the in situ setup. In contrast, Figure 4e reveals a significant increase in the peak intensities at 1721, 1300, 900, and 1430 cm^{-1} , corresponding to the C=O stretching vibration and the out-of-plane and in-plane vibrations of –OH. Notably, within the initial 10 min, the infrared signal for C=O shows minimal change. The signals of these functional groups become evident during subsequent reaction. By 30 min, the appearance of –OH associated with carboxyl groups is observed, indicating that the previously accumulated C=O groups are further oxidized

to carboxylic acids. These findings suggest that there is an induction period for the conversion of PE to carboxylic acid, which may be caused by the slower chain initiation.

Based on these findings, we propose a mechanistic framework for the reaction pathway, illustrated in Figure 4f. The high-spin cobalt sites in LCO catalyze the rapid conversion of $^3\text{O}_2$ into $^1\text{O}_2$, which attacks the C–H bonds of PE, initiating hydrogen atom transfer (HAT) and the formation of carbon radicals.^[15,43] These radicals are subsequently captured by O_2 to form carbon peroxide intermediates, which undergo a series of transformations to give C–O radicals. Due to the asymmetric electron distribution in the C–C bonds of PE, these C–O radicals are highly susceptible to β -scission, yielding shorter carbon-chain radicals and aldehydes. The carboxylic acids are formed based on the oxidation of

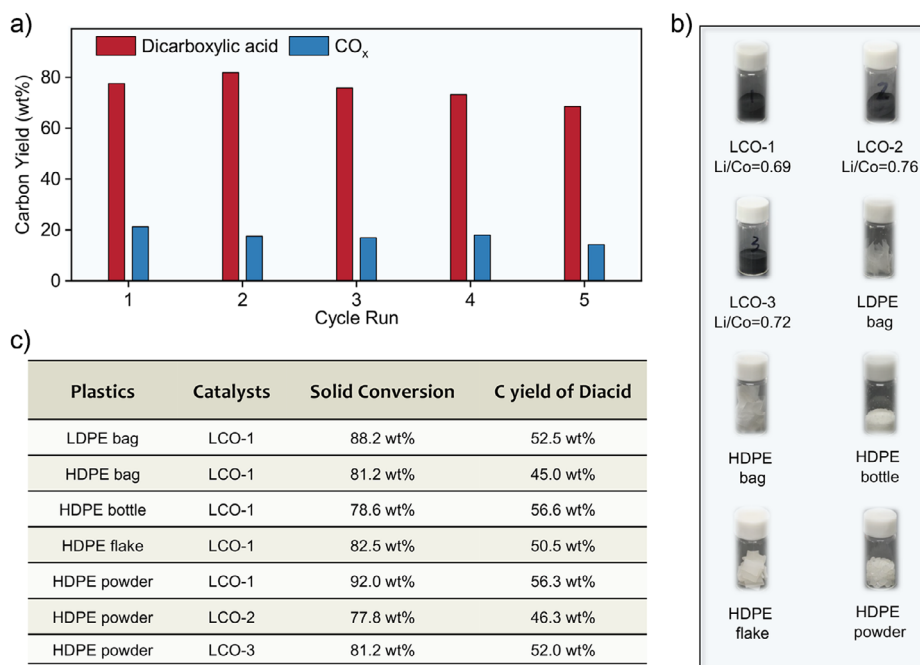


Figure 5. Demonstrations of upcycling of real-world waste PE. a) Catalytic stability performance diagram of $\text{Li}_{0.28}\text{CoO}_2$ catalyst during five cycles. Reaction conditions: $P(\text{O}_2) = 1.0 \text{ MPa}$, $T = 130^\circ\text{C}$, $t = 6 \text{ h}$, $m_{\text{catalyst}} = 20 \text{ mg}$, $m_{\text{PE}} = 200 \text{ mg}$. b) Digital images of various spent LCO cathode powders and real-world plastics. c) Summary of the catalytic performances for upcycling various real-world waste PE using spent LCO cathodes. Reaction conditions: $P(\text{O}_2) = 1.0 \text{ MPa}$, $T = 130^\circ\text{C}$, $t = 6 \text{ h}$, $m_{\text{catalyst}} = 20 \text{ mg}$, $m_{\text{PE}} = 200 \text{ mg}$.

aldehydes. Notably, β -scission can occur at both termini of the polymer chain, resulting in dicarboxylic acids.

Demonstration

The recyclability of the catalyst is a crucial factor for its potential industrial application. To ensure reliable results, the solid residue from each reaction was thoroughly washed with hot toluene to remove any residual unreacted PE, which could otherwise interfere with subsequent analyses. The recovered $\text{Li}_{0.28}\text{CoO}_2$ catalyst was then dried and reused in further cycle testing. As shown in Figure 5a, we conducted five consecutive cycles to evaluate the catalyst's stability and performance. Over these five cycles, the solid conversion rate exhibited only a minor decline, remaining consistently around 80.0 wt%. Moreover, the composition and ratio of the liquid products remained unchanged (Figure S18), where the liquid products were predominantly composed of C_4 – C_{10} dicarboxylic acids, consistently accounting for 65.0–80.0 wt% of the total liquid yield across all cycles. The morphology (Figure S19) and crystal structure (Figure S20) of used catalysts have slightly changes, which suggest excellent overall stability throughout the cycling tests. These findings underscore the robustness of the catalyst and its suitability for prolonged use in industrial applications.

Considering the universality of waste battery recycling, we evaluated the catalytic performance of different recycled LCO samples, designated as LCO-1/2/3. The Li/Co ratios of the three LCO-based catalysts, measured by ICP-OES, are listed in Figure 5b and Table S5. XRD analysis (Figure

S21) confirmed that all samples retained the characteristic LCO crystal structure. The (003) peak at $2\theta = 19^\circ$ and the (101) and (104) peaks at $2\theta = 37^\circ$ and 44.5° reflected that the spent LCO conformed to the typical $R\bar{3}m$ space group.^[39,44] The catalytic activity of the recycled LCO samples was evaluated in the oxidation of HDPE powder, with the results presented in Figure 5c. Although all three LCO samples exhibited strong catalytic activity, performance variations were observed among the samples. Specifically, the dicarboxylic acid carbon yields of LCO-1, LCO-2, and LCO-3 reached 56.3, 46.3, and 52.0 wt%, respectively (Figure S22). The differences in catalytic performance may be attributed to the changes in the Li/Co ratio, where lower Li/Co ratios lead to higher catalytic performance. These results again highlight the advantages of directly using waste LCO as a catalyst.

Real-world plastics often contain additives such as antioxidants, which may interfere with subsequent oxidation catalysis. To evaluate the robustness of the catalytic system, we used waste LCO-1 as a model catalyst to investigate its performance on a variety of commercially available PE plastics, including plastic bags, commercial plastic flakes, and plastic bottles. As shown in Figures 5c and S23, despite the presence of antioxidants and other additives in commercial plastics, LCO-1 exhibited excellent catalytic activity. The dicarboxylic acid carbon yield consistently remained around ~50.0 wt%, which was only slightly lower than the yield observed for pure HDPE powder. This slight reduction in yield may be attributed to the competitive oxidation of antioxidants, which could temporarily inhibit the oxidative cleavage of PE chains. Interestingly, commercial plastics demonstrated higher CO_x yields compared to pure plastics

(Table S6), likely due to the over-oxidation of antioxidants and other reactive components during the catalytic process. This observation suggests that additives in real-world plastics might influence the oxidation pathways, leading to enhanced formation of gaseous byproducts. Overall, the waste LCO catalyst demonstrates universal applicability in addressing real-world PE waste challenges.

Conclusion

In summary, we propose a green and sustainable co-recycling strategy for PE and LCO cathodes, in which spent cathode materials serve directly as effective catalysts for PE oxidation. This approach enables the upcycling of real-world PE waste into high-value dicarboxylic acids, addressing key challenges in plastic and battery waste management. Through comprehensive mechanistic studies, we demonstrate that the oxidation process is driven by high-spin Co^{3+} , which facilitates the generation of singlet oxygen. This reactive species initiates a HAT mechanism, allowing PE to be selectively converted into valuable chemical products. The proposed strategy not only provides a pathway for recycling complex waste streams but also delivers substantial economic benefits, aligning with global efforts toward a circular economy. We acknowledge that product separation remains a critical challenge in oxidative upcycling processes, particularly when dealing with complex plastic mixtures and diverse oxidation products. While some separation techniques (e.g., chromatography) are effective in laboratory settings, industrial-scale processes require cost-effective and energy-efficient alternatives, such as phase separation and reactive distillation. The scalability of this approach should be explored, particularly in its adaptability to other types of plastics and batteries.

Acknowledgements

This work was supported by the National Natural Science Foundation of China (22376152, 22208365, 52403139), Jiangsu Provincial Fund for Excellent Young Scholars (BK20240154), Natural Science Foundation of Jiangsu Province (BK20220298), and Suzhou Frontier Technology Research Advanced Materials Project (SYG202305). J.C. thanks the support from the Suzhou Key Laboratory of Advanced Photonic Materials, Suzhou Key Laboratory of Functional Nano & Soft Materials, Collaborative Innovation Center of Suzhou Nano Science & Technology, the 111 Project. The authors thank Du Chen, Zhongyu Li, and Chengxu Li from Soochow University for the help with GC-MS, XAS, and in situ FTIR characterizations. The authors acknowledge Mr. Binglei Jiao for his help with disassembling of LCO batteries.

Conflict of Interests

The authors declare no conflict of interest.

Data Availability Statement

The data that support the findings of this study are available from the corresponding author upon reasonable request.

Keywords: Chemical oxidation • Dicarboxylic acid • Lithium ions battery • Polyethylene recycling • Spent LiCoO_2

- [1] C. Ostle, R. C. Thompson, D. Broughton, L. Gregory, M. Wootton, D. G. Johns, *Nat. Commun.* **2019**, *10*, 1622.
- [2] K. Lee, Y. Jing, Y. Wang, N. Yan, *Nat. Rev. Chem.* **2022**, *6*, 635–652.
- [3] A. Rahimi, J. M. García, *Nat. Rev. Chem.* **2017**, *1*, 0046.
- [4] A. Singh, N. A. Rorrer, S. R. Nicholson, E. Erickson, J. S. DesVeaux, A. F. T. Avelino, P. Lamers, A. Bhatt, Y. Zhang, G. Avery, L. Tao, A. R. Pickford, A. C. Carpenter, J. E. McGeehan, G. T. Beckham, *Joule* **2021**, *5*, 2479–2503.
- [5] R. Geyer, J. R. Jambeck, K. L. Law, *Sci. Adv.* **2017**, *3*, e1700782.
- [6] W. Zhang, S. Kim, L. Wahl, R. Khare, L. Hale, J. Hu, D. M. Camaioni, O. Y. Gutiérrez, Y. Liu, J. A. Lercher, *Science* **2023**, *379*, 807–811.
- [7] F. Zhang, M. Zeng, R. D. Yappert, J. Sun, Y.-H. Lee, A. M. LaPointe, B. Peters, M. M. Abu-Omar, S. L. Scott, *Science* **2020**, *370*, 437–441.
- [8] L. Gan, Z. Dong, H. Xu, H. Lv, G. Liu, F. Zhang, Z. Huang, *CCS Chem.* **2023**, *6*, 313–333.
- [9] B. Zhao, Z. Hu, Y. Sun, R. Hajiayi, T. Wang, N. Jiao, *J. Am. Chem. Soc.* **2024**, *146*, 28605–28611.
- [10] Q. Kang, M. Chu, P. Xu, X. Wang, S. Wang, M. Cao, O. Ivasenko, T.-K. Sham, Q. Zhang, Q. Sun, J. Chen, *Angew. Chem. Int. Ed.* **2023**, *62*, e202313174.
- [11] M. Chu, X. Wang, X. Wang, P. Xu, L. Zhang, S. Li, K. Feng, J. Zhong, L. Wang, Y. Li, L. He, M. Cao, Q. Zhang, L. Chi, J. Chen, *J. Am. Chem. Soc.* **2024**, *146*, 10655–10665.
- [12] O. Guselnikova, O. Semyonov, E. Sviridova, R. Gulyaev, A. Gorbunova, D. Kogolev, A. Trelin, Y. Yamauchi, R. Boukherroub, P. Postnikov, *Chem. Soc. Rev.* **2023**, *52*, 4755–4832.
- [13] M. Chu, W. Tu, S. Yang, C. Zhang, Q. Li, Q. Zhang, J. Chen, *SusMat* **2022**, *2*, 161–185.
- [14] K. D. Nixon, Z. O. G. Schyns, Y. Luo, M. G. Ierapetritou, D. G. Vlachos, L. T. J. Korley, I. I. I. Epps, *Nat. Chem. Eng.* **2024**, *1*, 615–626.
- [15] S. Oh, E. E. Stache, *Chem. Soc. Rev.* **2024**, *53*, 7309–7327.
- [16] K. P. Sullivan, A. Z. Werner, K. J. Ramirez, L. D. Ellis, J. R. Bussard, B. A. Black, D. G. Brandner, F. Bratti, B. L. Buss, X. Dong, S. J. Haugen, M. A. Ingraham, M. O. Konev, W. E. Michener, J. Miscall, I. Pardo, S. P. Woodworth, A. M. Guss, Y. Román-Leshkov, S. S. Stahl, G. T. Beckham, *Science* **2022**, *378*, 207–211.
- [17] R. Cao, M.-Q. Zhang, C. Hu, D. Xiao, M. Wang, D. Ma, *Nat. Commun.* **2022**, *13*, 4809.
- [18] X. Wei, Q. Zhang, C. Shen, X. Zhao, F. Zhang, X. Liu, G. Wu, S. Xu, Y.-Z. Wang, *Mater. Horiz.* **2023**, *10*, 3694–3701.
- [19] Z. Huang, M. Shanmugam, Z. Liu, A. Brookfield, E. L. Bennett, R. Guan, D. E. Vega Herrera, J. A. Lopez-Sanchez, A. G. Slater, E. J. L. McInnes, X. Qi, J. Xiao, *J. Am. Chem. Soc.* **2022**, *144*, 6532–6542.
- [20] N. E. Munyaneza, R. Ji, A. DiMarco, J. Miscall, L. Stanley, N. Rorrer, R. Qiao, G. Liu, *Nat. Sustain.* **2024**, *7*, 1681–1690.
- [21] P. Hu, C. Zhang, M. Chu, X. Wang, L. Wang, Y. Li, T. Yan, L. Zhang, Z. Ding, M. Cao, P. Xu, Y. Li, Y. Cui, Q. Zhang, J. Chen, L. Chi, *J. Am. Chem. Soc.* **2024**, *146*, 7076–7087.
- [22] H. Ran, S. Zhang, W. Ni, Y. Jing, *Chem. Sci.* **2024**, *15*, 795–831.

- [23] B. Zhao, H. Tan, J. Yang, X. Zhang, Z. Yu, H. Sun, J. Wei, X. Zhao, Y. Zhang, L. Chen, D. Yang, J. Deng, Y. Fu, Z. Huang, N. Jiao, *Innovation* **2024**, *5*, 100586.
- [24] Z. Xu, N. E. Munyaneza, Q. Zhang, M. Sun, C. Posada, P. Ventura, N. A. Rorrer, J. Miscall, B. G. Sumpter, G. Liu, *Science* **2023**, *381*, 666–671.
- [25] K. Wang, R. Jia, P. Cheng, L. Shi, X. Wang, L. Huang, *Angew. Chem. Int. Ed.* **2023**, *62*, e202301340.
- [26] Q. Zhang, J. He, X. Wei, C. Shen, P. Ye, W. An, X. Liu, H. Li, S. Xu, Z. Su, Y.-Z. Wang, *Angew. Chem. Int. Ed.* **2024**, e202407510.
- [27] C. Bauer, S. Burkhardt, N. P. Dasgupta, L. A.-W. Ellingsen, L. L. Gaines, H. Hao, R. Hischer, L. Hu, Y. Huang, J. Janek, C. Liang, H. Li, J. Li, Y. Li, Y.-C. Lu, W. Luo, L. F. Nazar, E. A. Olivetti, J. F. Peters, J. L. M. Rupp, M. Weil, J. F. Whitacre, S. Xu, *Nat. Sustain.* **2022**, *5*, 176–178.
- [28] M. Liu, T.-C. Yang, Z. Pan, J. Lee, L. An, B. Qiu, H. Yin, C.-M. Yang, L. Y. S. Lee, *ACS Energy Lett.* **2023**, *8*, 1652–1661.
- [29] G. Harper, R. Sommerville, E. Kendrick, L. Driscoll, P. Slater, R. Stolkin, A. Walton, P. Christensen, O. Heidrich, S. Lambert, A. Abbott, K. Ryder, L. Gaines, P. Anderson, *Nature* **2019**, *575*, 75–86.
- [30] G. Ji, D. Tang, J. Wang, Z. Liang, H. Ji, J. Ma, Z. Zhuang, S. Liu, G. Zhou, H.-M. Cheng, *Nat. Commun.* **2024**, *15*, 4086.
- [31] Y. Tao, C. D. Rahn, L. A. Archer, F. You, *Sci. Adv.* **2021**, *7*, eabi7633.
- [32] Y.-C. Yin, C. Li, X. Hu, D. Zuo, L. Yang, L. Zhou, J. Yang, J. Wan, *ACS Energy Lett.* **2023**, *8*, 3005–3012.
- [33] X. Mu, K. Huang, G. Zhu, Y. Li, C. Liu, X. Hui, M. Sui, P. Yan, *Nano Energy* **2023**, *112*, 108465.
- [34] J. Wang, Z. Liang, Y. Zhao, J. Sheng, J. Ma, K. Jia, B. Li, G. Zhou, H.-M. Cheng, *Energy Storage Mater.* **2022**, *45*, 768–776.
- [35] X. Lou, P. Yan, B. Jiao, Q. Li, P. Xu, L. Wang, L. Zhang, M. Cao, G. Wang, Z. Chen, Q. Zhang, J. Chen, *Nat. Commun.* **2024**, *15*, 2730.
- [36] H. Lei, Z. Zeng, J. Li, X. Cui, B. Wang, Y. Shi, W. Sun, X. Ji, Y. Yang, P. Ge, *Adv. Funct. Mater.* **2024**, *34*, 2402325.
- [37] X. Zhao, C. Kuang, H. Liu, C. An, M. Wang, T. Mu, *ChemSusChem* **2024**, *17*, e202400105.
- [38] Z. Yao, T. Fu, T. Pan, Z. Jiang, X. Fan, S. Liu, Q. Guo, Y. Li, C. Zheng, W. Sun, *Adv. Funct. Mater.* **2024**, *34*, 2408152.
- [39] C. Lin, J. Li, Z. Yin, W. Huang, Q. Zhao, Q. Weng, Q. Liu, J. Sun, G. Chen, F. Pan, *Adv. Mater.* **2024**, *36*, 2307404.
- [40] T. Gan, X. Chen, X. Chu, P. Jing, S. Shi, Z. Zhang, W. Zhang, J. Li, S. Zhang, M. Pavanello, D. Wang, G. Liu, *J. Am. Chem. Soc.* **2024**, *146*, 16549–16557.
- [41] A. Grimaud, O. Diaz-Morales, B. Han, W. T. Hong, Y.-L. Lee, L. Giordano, K. A. Stoerzinger, M. T. M. Koper, Y. Shao-Horn, *Nat. Chem.* **2017**, *9*, 457–465.
- [42] W. Xie, Y. Zhang, H. Zheng, P. Lyu, X. Ke, T. Li, H. Fang, Y. Sun, J. Dong, L. Lin, C. Wang, X. Tang, *ACS Catal.* **2024**, *14*, 17510–17524.
- [43] S. Oh, H. Jiang, L. H. Kugelmass, E. E. Stache, *ACS Cent. Sci.* **2025**, *11*, 57–65.
- [44] M. Zan, H. Xie, S. Jiao, K. Jiang, X. Wang, R. Xiao, X. Yu, H. Li, X. Huang, *Small Sci.* **2024**, 2400162.

Manuscript received: January 18, 2025

Revised manuscript received: April 01, 2025

Accepted manuscript online: April 14, 2025

Version of record online: April 25, 2025